

EXPERIMENTAL STUDY OF THE REATTACHMENT
PRESSURE RISE AT SUBSONIC SPEEDS

Thesis by
Jark Chong Lau

In Partial Fulfillment of the Requirements
For the Degree of
Aeronautical Engineer

California Institute of Technology
Pasadena, California

1965

(Submitted August 20, 1964)

ACKNOWLEDGEMENTS

The author wishes to express his deep appreciation to Dr. A. Roshko for the advice and guidance received through the course of this work.

It is also with gratitude that he acknowledges the help of Mrs. Geraldine Krentler in the preparation of this script.

Thanks are also due to the staff of the Guggenheim Aeronautics Laboratory, and in particular, to Messrs. Lewis Balthasar and Ray Wagoner for their assistance in the course of the investigation.

Finally the author wishes to thank the California Institute of Technology and the Singapore Polytechnic for the opportunity to study in this Institute and the financial assistance received.

ABSTRACT

An experimental study was made of the problem of separated flow with reattachment at subsonic speeds in various geometrical configurations. It was found that when the boundary layer thickness at separation was small, the values of the reattachment pressure rise coefficient agreed with those from the Korst-Chapman theory. The importance of the relative positions of the transition and reattachment was investigated. In the free shear layer, transition occurred at Reynolds numbers as low as 3×10^3 , based on distance from the separation point.

TABLE OF CONTENTS

PART	TITLE	PAGE
	Acknowledgments	ii
	Abstract	iii
	Table of Contents	iv
	Notation and Definitions	v
	List of Figures	viii
1.	Introduction	1
2.	Theory	3
3.	Description of Apparatus and Experimental Techniques	9
4.	Results and Discussion	17
	Smoke Pictures	17
	Reattachment Pressure Distributions	18
	Reattachment Pressure Rise (Recovery)	
	Rise Coefficient, σ	24
	Effect of Reynolds Number	27
	Transition Reynolds Number	28
5.	Conclusion	31
	References	33
	Figures	35

NOTATION AND DEFINITIONS

- b = $\frac{1}{2}$ base height of models
 C_p = pressure coefficient = $\frac{p - p_\infty}{\frac{1}{2} \rho U_\infty^2}$
 \tilde{C}_p = reduced pressure coefficient = $\frac{p - p_1}{\frac{1}{2} \rho U_1^2} = \frac{C_p - C_{p1}}{1 - C_{p1}}$
 d = $\frac{1}{2}$ frontal height of models (= b in most models)
 h = step height
 p = pressure
 Re = Reynolds Number
 r = distance between the separation and reattachment points
 t = distance between the separation and transition points
 U_1 = velocity at edge of free shear layer
 u_1 = velocity at a point in the free shear layer
 x = distance measured from the separation point
 δ_s = boundary layer thickness at the separation point
 σ = pressure rise (or recovery) coefficient

Subscript and Superscript

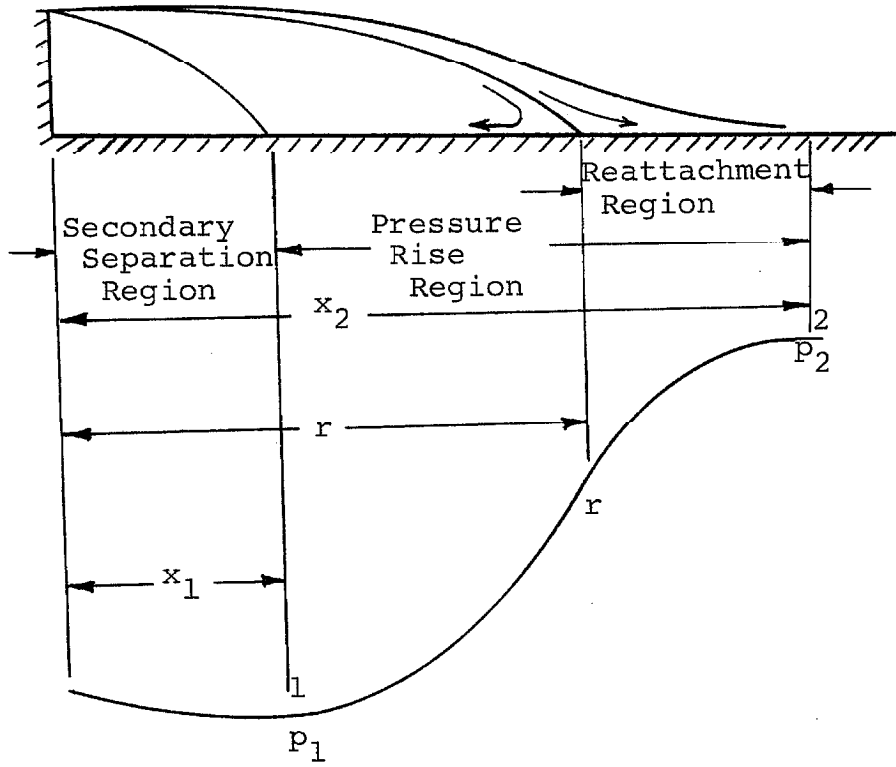
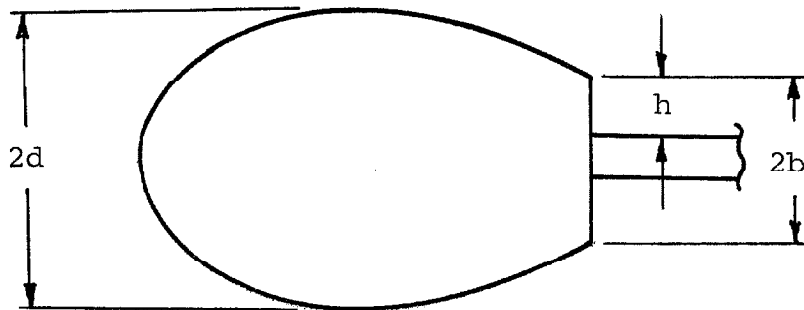
- ∞ = free stream conditions
 1 = minimum pressure location
 2 = maximum pressure location
 r = reattachment point

NOTATION AND DEFINITIONS (Con't)

- s = separation point
- o = total conditions
- * = dividing streamline conditions

DEFINITIONS

Potential Flow Region

Reattachment Zone

LIST OF FIGURES

FIGURE		PAGE
1.	Forebody Shapes	35
2.	Pressure Plate	37
3.	Smoke Pictures Showing Transition	38
4.	Reattachment Pressure Distribution	42
5.	Reattachment Pressure Distribution	43
6.	Reattachment Pressure Distribution	44
7.	Reattachment Pressure Distribution	45
8.	Reattachment Pressure Distribution	46
9.	Reattachment Pressure Distribution	47
10.	Reattachment Pressure Distribution	48
11.	Comparison of Results of Figure 10 with Tani's (Ref. 11)	48
12.	Comparison of Results for Various Shapes (x normalized by $\frac{1}{2}$ frontal height)	49
13.	Comparison of Results for Various Shapes (x normalized by step height)	50
14.	Comparison of Results for 1-inch Plate	51
15.	Reattachment Pressure Distribution in Reduced Coordinates	52

1. INTRODUCTION

The problem of separated flow has engaged the energies of scientists and engineers through the ages.

By and large, this problem may be broken up into two parts. The first deals with flows where the separated streamline does not reattach onto a solid boundary. This is in general an unsteady flow configuration and may result in the generation of the famous Kármán vortex street. The second deals with separated flows which reattach, and are, in general, steady; it is on the investigation of this part of the problem that is undertaken in the present work.

The problem of separated flows with reattachment is a long standing one. It probably appeared when running water first attracted the fascination of Man, and has held an important place in all forms of hydraulic design. However, the great impetus to derive a fuller understanding of this phenomenon probably came with the airplane. Of late, this problem has established for itself a prominent position in the study of roughness effect on boundary layer.

One of the simplest forms of the problem is a step in the tunnel wall. However, for a basic investigation, this has the disadvantage that there is always a boundary layer at the point of separation, which may be very thick.

To reduce this, one needs a body with a relatively short distance from leading edge to step. This may be achieved by having a bluff body with splitter plate behind it. Such a setup was adopted in this investigation, with several bluff body (henceforth called forebody) shapes being used.

The understanding of the whole problem of separated flow with reattachment has been enriched by the independent works of Korst, Page, and Childs (Refs. 1, 2) and Chapman, Kuehn, and Larson (Ref. 3), in transonic and supersonic flow. They postulated a criterion from which they obtained explicit equations relating the base and peak pressures in the reattachment zone. There seems no reason why the same criterion may not be applied to subsonic cases. One of the purposes of the present investigation was to determine where this is indeed true.

In the problem of flow separation and reattachment, the role of transition to turbulence may be very important. In particular, the location of the transition point with respect to reattachment point is significant. This was investigated in the present experiments.

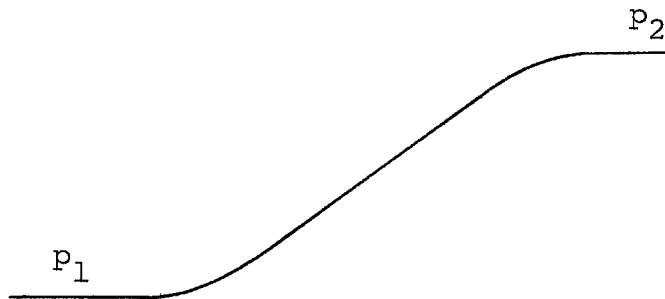
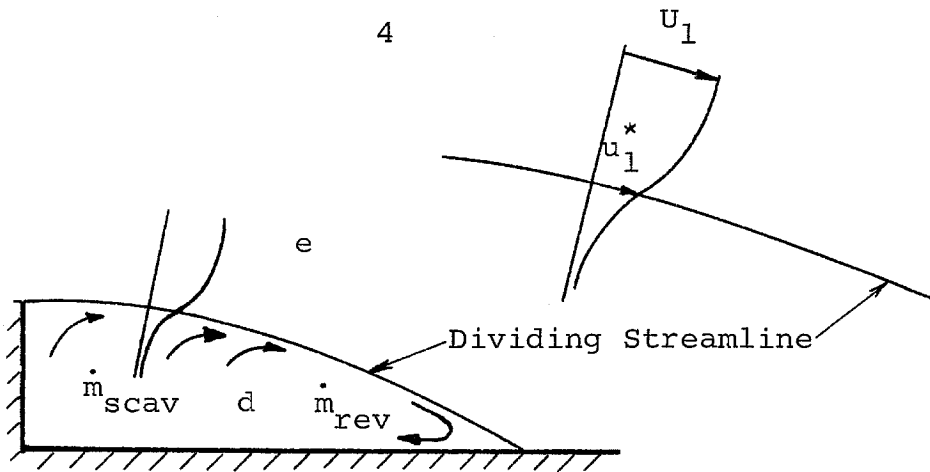
2. THEORY

Major contributions to the theoretical study of separated flows with reattachment have come from Korst, Page, and Childs (Refs. 1, 2), and Chapman, Kuehn, and Larson (Ref. 3). The former attacked the problem from the standpoint of a fully turbulent free shear layer, while the latter, that of a fully laminar free shear layer. Both of them adopted a similar model, and one outstanding result of their approach is that it allows the calculation of the base pressure without resort to empirical means.

In essence, the basis for this model hinges on the idea that, at equilibrium, $\dot{m}_{scav.}$, the mass rate of air scavenged from the dead air region (designated "d" in sketch 1) is balanced by $\dot{m}_{rev.}$, the mass rate returned to it.

This leads to a criterion which gives an explicit equation for finding the base pressure, p_1 , if the peak pressure, p_2 , in the reattachment region is known; or vice versa.

The criterion (see sketch 1), given independently by Korst and Chapman, states that, in view of the assumptions of the model, there must be a streamline isolating the dead air region, d, from the external flow, e. Moreover, the total pressure, p^0 , on this dividing streamline must be equal to the peak reattachment pressure, p_2 . Then, using



Sketch 1

the boundary layer theory assumption that the pressure is constant across the free shear layer, we have¹:

$$\begin{aligned}
 p_2 = p^0 &= p_1 + \frac{1}{2} \rho u_1^{*2} \\
 &= p_1 + \frac{1}{2} \rho U_1^2 \left(\frac{u_1^*}{U_1} \right)^2
 \end{aligned}$$

or

$$\tilde{C}_{p \max} = \frac{p_2 - p_1}{\frac{1}{2} \rho U_1^2} = \left(\frac{u_1^*}{U_1} \right)^2 \quad (1)$$

1. The analysis and form of the final equation are different from those of Korst et. al., or Chapman et. al., but the idea is the same.

This pressure coefficient is defined with respect to conditions (p_1 , U_1 , etc.) along the constant pressure portion of the free shear layer. To relate it to free stream conditions, we also have:

$$\begin{aligned} \frac{p_2 - p_1}{\frac{1}{2} \rho U_1^2} &= (C_{p_2} - C_{p_1}) \left(\frac{U_\infty}{U_1} \right)^2 \\ &= \frac{C_{p_2} - C_{p_1}}{1 - C_{p_1}} \end{aligned}$$

($\left(\frac{U_1}{U_\infty} \right)^2 = 1 - C_{p_1}$, from Bernoulli's Equation)

$$\therefore \tilde{C}_{p \text{ max}} = \frac{C_{p_2} - C_{p_1}}{1 - C_{p_1}} = \left(\frac{u^*}{U_1} \right)^2 \quad (2)$$

Using mixing length theory for laminar mixing layers with zero boundary layer thickness at separation, Chapman (Ref. 4) derived the value of 0.587 for $\frac{u^*}{U}$. Korst et. al. (Ref. 2), on the other hand obtained 0.62 for the case of a fully developed incompressible turbulent flow profile.

$$\therefore \tilde{C}_{p \text{ max}} = \begin{array}{ll} 0.345 & \text{pure laminar (Chapman)} \\ 0.385 & \text{pure turbulent (Korst)} \end{array}$$

No special significance should be attached to the difference in the values for these two cases. Korst's value is obtained by approximating the turbulent profile by an error function. If the more exact profile from

Görtler's constant eddy viscosity theory is used, then the same value, 0.345, as in the laminar theory is obtained.

The basic assumptions of the model may be summarized as follows:

(a) The free streamline separates from a sharp edge or a point where the boundary thickness is zero. (If this were not so, the value of $\frac{u^*}{U}$ and consequently of $\tilde{C}_p \max$ would be less than those prescribed.)

(b) The separated free shear layer is either purely laminar or purely turbulent. No allowance is made for a case with transition occurring in the layer.

The importance of the relative positions of the transition and reattachment locations was qualitatively explained by Chapman. The gist of the conclusions may be stated as follows:

when the transition is close to the reattachment region, changes in Reynolds number will affect the flow characteristics substantially; but with the transition closer to the separation point, Reynolds number effects are very small.

Many investigators, studying the airfoil leading edge stall problem at subsonic speeds (e.g., Crabtree (Refs. 5, 6), and Moore (Refs. 7, 8)), have reported on

the significance of a parameter, σ , defined exactly as $\tilde{C}_{p \max}$ above. However, the Korst-Chapman theory has not been identified with these findings, and these two lines of research have been following independent paths so far. The probable reason is that the Korst-Chapman theory has been "traditionally" devoted to transonic and supersonic problems. In any case, a comparison of the results of the two approaches reveal surprising agreement. For instance, Moore (Ref. 7), working with short separation bubbles on plates having airfoil shapes faired to the leading edge, found that the value of σ increased with increase in angle of attack, reaching a maximum of about 0.36. Beyond this, further increase in the angle of attack would result in either a long bubble or stall. (In the opinion of this author, the increase in σ is not so much due to the increase in the "back pressure" when the angle of attack is increased as the decrease in the boundary layer thickness at separation.)

These results lend support to the validity of the Korst-Chapman theory in the subsonic speed range, and suggest that $\tilde{C}_{p \max}$ (or σ) is a useful parameter for all subsonic, reattaching flows.

In summary, the salient points are stated as follows:

- (a) In any case where the separated flow reattaches,

the maximum possible value of σ is about 0.36.

(b) If the boundary layer thickness at separation is zero, the maximum value of σ should be attained.

(c) If the boundary layer thickness is finite at the point of separation, the value of σ is less than the maximum; the thicker the boundary layer for a given geometrical configuration, the lower will be the value of σ .

3. DESCRIPTION OF APPARATUS AND EXPERIMENTAL TECHNIQUES

Wind Tunnel

The experiments were conducted in the GALCIT 20- by-20-inch low turbulence wind tunnel. A detailed description of it may be found in reference 9.

The wind speeds available in this tunnel range from about 1.5 feet per second (45 cm. per sec.) to 50 feet per second (1520 cm. per sec.). The turbulence level is about 0.03%.

Traversing Mechanism

The pitot tube and hot-wire probes used during any part of the experiment were supported from the ceiling of the working section by the traversing mechanism. This permitted vertical and longitudinal (flow direction) positioning of the probes. Measurements of the longitudinal positions were accurate to 0.01 inch, while those of the vertical position to 0.005 inch.

The traversing mechanism was removed when only static pressures were taken and when the visual techniques were used.

Forebodies (or Models)

The shapes of the forebodies investigated are shown in figure 1. These shapes were chosen because they include

the full range of flow configurations likely to be encountered in practice.

The forebodies were attached symmetrically to the pressure plate to form an integral assembly.

Pressure Plate

An assembly drawing of the pressure plate is shown in figure 2. It was supported horizontally at the middle of the working section and midway between the ceiling and floor of the tunnel. It acts like a splitter plate (Ref.10), isolating the two free shear layers separating from the edges of the forebody.

An important requirement of this plate is that it must be as flat as feasible in manufacture. It is useful to have it as thin as possible, but it must be able to support its own weight and that of the forebodies without distortion also. The thickness used was 5/16 inch. As the name implies, the plate was designed to measure the distribution of static pressure acting on it.

Several methods of construction were considered which would have resulted in thinner plates. One of them was to recess grooves in the plate, inlaying same with tubes, and then levelling the surface off with a hard plastic or metallic bonding compound such as Epoxy or Devcon. This is quite a standard practice under other circumstances.

However, it was felt in this case that, with a plate of this size, any machining to put long grooves on a thin plate would result in warpage. Another one of the seriously considered methods was to lay the tubes on a very thin plate, and then build up the surface with bonding compound. Besides being very expensive, this method seemed to be too "permanent" and inflexible to allow future alterations.

The construction finally adopted consisted of a 21" x 10" x $\frac{1}{8}$ " flat ground steel plate with brass tubes soldered to one of its surfaces. The plate was used in the stock condition without further machining in order to preserve the flatness, and brass tubes (which extended beyond the length of the plate) were soldered onto the plate with solder having a low melting point, to minimize thermal distortions. The pressure orifices were then drilled right through the plate and tube wall. (Special care was taken when soldering to ensure complete sealing of the tube-plate contact surface in this region.) Over the tubes, a thin bakelite sheet was fastened to form the other flat surface of the pressure plate. The steel strips fastened along the front and back edges of the steel plate were provided with tapped holes by which a forebody could be held to the pressure plate.

The leading and trailing edges of the plate were interchangeable. The choice of its actual orientation in

the tunnel depended on the point of reattachment. For example, the side with the tubes closer together was placed downstream in the case of the 1-inch plate; and the reverse when the $\frac{1}{2}$ -inch plate was used.

Pressure Measurement

Pressures were measured with a micro-manometer having an accuracy of about 0.02 millimeters of manometer fluid. To measure the static pressure on the plate, the appropriate orifice on the plate was connected to one leg of the manometer. A pitot tube, mounted on the traversing mechanism, measured the pitot pressure.

Velocity Measurement

The velocity in the working section was obtained using a method reported by Roshko (Ref. 9). It works on the principle that, for a given circular cylinder and under a given set of atmospheric conditions, the shedding frequency of vortices is related to the air speed.

A $\frac{1}{8}$ -inch diameter rod was placed upstream of the working section of the tunnel with a hot-wire positioned to pick up signals of vortices shed. This constituted the velocity measuring device. The device was calibrated to give the air speed at the working section. For the high speed range, the yardstick for the calibration consisted of

a standard pitot-static probe placed at the working section. At low speeds, when the low dynamic heads rendered measurements of pitot-static pressure differences inaccurate, a "bootstrap" method, using a secondary system of circular cylinder and hot-wire pick-up placed at the working section, was employed.

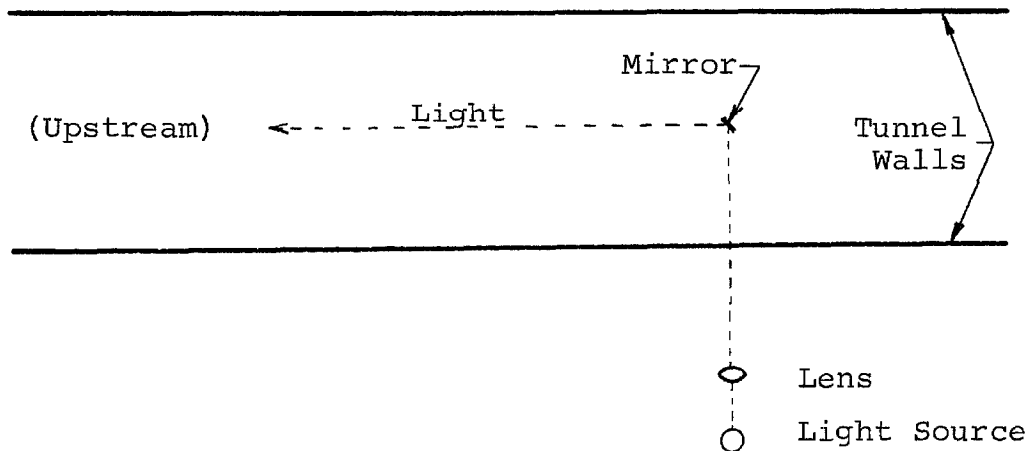
Transition Location

The location of the transition in the separated flow was found by means of the smoke technique. A smoke filament was introduced at the leading edge of the models. Wherever possible and convenient (e.g., 1-inch plate and semicircular cylinder), the smoke tube was inlaid and sealed flush in a groove in the back of the model, and connected to a hole drilled from the leading edge of the model through which the smoke issued. For other models, smoke was brought in through a 3/64-inch O.D. steel tube laid along the leading edge.

The smoke generator was of a standard type taken out of a demonstration model smoke tunnel. It consists of a heating element on which kerosene may be dropped at regulated intervals, and there is provision for pressurizing the smoke chamber if needed.

The light source was a 6-volt microscope illuminator lamp operating at 15 amps. Its strip filament and a lens

produced a narrow beam which was reflected upstream off a little mirror placed in the tunnel far downstream of the pressure plate. A schematic view of the arrangement is shown in sketch 2. The arrangement was adjusted to



Sketch 2

concentrate as much light as possible on the separated smoke filament without resulting in too much glare reflected from the pressure plate. The pictures were recorded on Polaroid 3000 film, and exposure times ranged from about 8 seconds to 2 minutes at an aperture setting of 4.7.

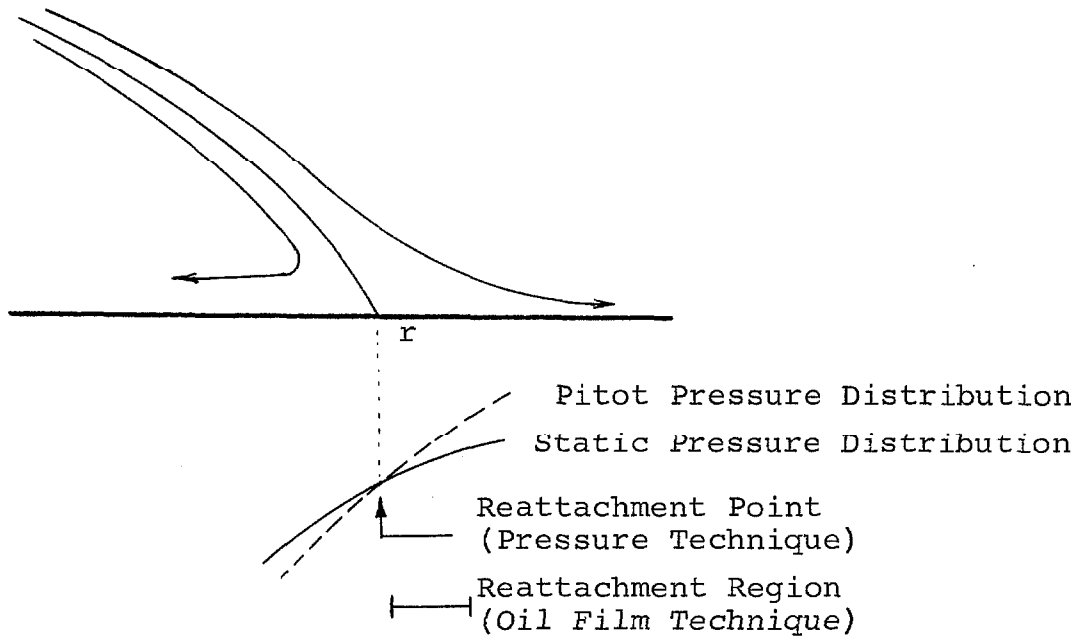
The pressure distribution was found to alter by a negligible amount when smoke was introduced.

The transition location so obtained was checked with a hot-wire.

Reattachment Location

The reattachment point is defined as the point at which the surface flow reverses in direction.

Static and pitot pressures along the pressure plate were taken consecutively, with the pitot reading one step (or $\frac{1}{4}$ to $\frac{1}{2}$ inch) behind the static. The pitot tube was displaced about 1 inch laterally from the line of the static pressure orifices on the pressure plate. Typical pressure distributions are shown in sketch 3. The point of inter-



Sketch 3

section of the two curves determined the reattachment point. As the angle of intersection of these two curves was very small generally, it was found more convenient to plot the differences in the two pressures, defining the reattachment point by the location at which the curve crossed the abscissa. This latter approach gave better definition.

Another method for locating the reattachment region was to observe the surface flow direction by means of an oil film. A thin film of oil and kerosene mixed with a suspension of aluminium pigment was smeared on the surface of the pressure plate. In the region where the surface flow alternated in direction, a faint collection of the pigment was noticed. This was taken to be the reattachment region.

The reattachment region found from the oil film technique was generally just downstream of the reattachment point found using the pitot-static technique. Their relative positions are shown in sketch 3.

4. RESULTS AND DISCUSSION

Smoke Pictures

The smoke pictures in figure 3 give a visual view of the character of the free streamlines separating from seven of the forebodies. They were taken at three tunnel speeds.

These pictures were taken with the camera mounted close to one side of the tunnel, and therefore are perspective in nature.

The line of light extending from the left hand side of each picture shows the narrow strip of the pressure plate which was illuminated by the light directed upstream. The upper streak line represents the actual free streamline separating from the forebody, and the lower, the reflection in the pressure plate. It may be seen that the base of the model was reflected in the same way. (A flat black paint was sprayed on the back of each model to minimize glare from it but this was not very successful.)

The transition is indicated by the point at which the cross section of the smoke filament suddenly starts to increase. At each position of the camera and arrangement of the lighting, a picture was taken of a scale placed along the line where the smoke had passed. By comparison with the smoke picture, a determination of the transition distance could be made.

A study of these pictures shows two contrasting patterns of flow differentiated by the relative distance between the transition and the reattachment region. Figure 3(a), (b), (c), (d), and (e) come under one category where the transition is far from the reattachment. In these cases, although changes in transition location may be observed when the speed is altered, the changes are small, and the general flow field remains relatively unaffected. On the other hand, when the transition is close to the reattachment, as in figure 3(f), and (g) (the second category), changes in speed are accompanied by appreciable changes in the distances of the transition and reattachment locations. It is seen that the separation bubble then actually shortens with increase in speed.

Reattachment Pressure Distributions

The reattachment pressure distributions along the pressure plate for seven of the forebody shapes investigated are shown in figures 4 to 10. These data were obtained for three air speeds in each case. As the purpose of these experiments was to observe the reattachment phenomenon of a separated free shear layer, particularly in the different pressure fields produced by rather arbitrary geometrical configurations, it was of no interest to adjust the pressure readings to account for tunnel wall effects.

The pressures are presented as $C_p (= \frac{p - p_\infty}{\frac{1}{2} \rho U_\infty^2})$, while the distances along the pressure plate (measured from the separation points) are normalized by one-half of the base height (see "NOTATION AND DEFINITIONS").

Figures 12 and 13 contain pressure plots for all shapes at a speed of 29.5 feet per second. The distances of the former are normalized by one-half the frontal height; and the latter by the step height.

In very broad terms, the curves in figures 4 to 10 may be put into two classes -- ones that are not affected by the change in speed, and the others showing alteration of the curves both in shape and position when the speed is changed. This classification coincides with the two categories observed from the smoke pictures. Figures 4 to 8 belong to the first class, and figures 9 and 10 the other.

Figures 4 to 6 represent a sequence of configurations, having square fronts facing the oncoming fluid, in which the step heights are progressively decreasing. The last figure is for the limiting case of zero step height. These curves also represent flows with very small boundary layer thicknesses at separation. The length of the reattachment zone for these models, when normalized by one-half of the frontal height, decreases in the same sequence as the step heights. (In physical length, the order of the last two models is interchanged.) This is best illustrated in figure 12.

It may be seen that the minimum pressures on the pressure plots of figures 4 and 5 (1- and $\frac{1}{2}$ -inch plates respectively) are approximately the same, and, although the curves of figure 4 have not reached a maximum before the trailing edge of the plate, the tendency indicates that the peak pressures are very nearly the same too.

In figure 6 (flat nose plate), the maximum and minimum pressures are much lower than for the configurations of figures 4 and 5. The whole pressure level is lowered; in fact, these pressures were the lowest measured throughout these experiments. The important difference in this model is that the plate was 1 inch thick instead of $\frac{5}{16}$ inch, as for all the others. The base pressure on its flat trailing edge was undoubtedly lower than for the thin plate, and, of course, its effect extended further upstream. This resulted in the pressure in the reattachment region being abnormally lowered, and, consequently, in the separation region also, since the reattachment pressure recovery coefficient, σ (see next section), is expected to be unchanged.

The pressure plots of figures 7 and 8 (truncated airfoil I and 1-inch semicircular cylinder) are very similar in their pressure levels and extent of the reattachment zone. (The pressure distributions for the configuration of figure 7 at the lower speeds are not much displaced from the curve shown and are therefore left out.)

In figure 7, the longitudinal distance is normalized by one-half the base height; but when it is normalized by one-half the frontal height instead, the curves for the two configurations draw closer yet (see figure 12). Therefore, although the geometrical shapes of these two models are generally different, their forward portions are very similar, and the influence that they have on the flow field is very alike. Also shown in figure 7 is the pressure distribution when a piece of No. 60 sandpaper was wrapped around the leading edge of the model. Without the sandpaper, separation was just ahead of maximum thickness (see Fig. 3(d)), while with sandpaper it was just ahead of the trailing edge. This explains the large change in pressure level, since a relatively large change in effective geometry occurs.

The similarity in the behavior of the curves in figures 9 and 10 ($\frac{1}{2}$ -inch semicircular cylinder and truncated airfoil II, respectively) has been pointed out. However, major differences between the two cases are also noticeable. One is that while maximum and minimum pressures of the curves in figure 9 show definite variation with speed, those of figure 10 are practically unchanged. Moreover, the pressures are vastly different in magnitude for the two cases. One fundamental difference between these two cases is the boundary layer thickness at separation, a subject

which will be discussed more fully in the following section. But, be that as it may, reference to figure 12 shows that the two sets of curves have the same gradients in the pressure rise region, and that this gradient is higher than for the other cases.

It was observed that the shapes of the pressure plots for the truncated airfoil II were very similar in all respects to those obtained by Tani (Ref. 11), and Moore (Ref. 8). This is because the configuration of this airfoil most closely resembles those used by Tani and Moore. For comparison, the curve for the highest speed ($U = 29.5$ feet per second) is plotted beside one of Tani's in figure 11. The two curves represent configurations having approximately the same ratios of boundary layer thickness of the separating flow to step height.

In table 1 are ratios of the distance of the transition (from the separation point), t , to the distances of the reattachment, r , and the peak pressure location, x_2 , respectively. Taking the first ratio as an example, it may be seen that the magnitudes of the ratios fall under the same classification as outlined above. Attempts to correlate these ratios with pressure data within each of the two categories to observe any possible trends were unsuccessful.

Moore (Ref. 8), Chapman et. al. (Ref. 3), and others

U(ft-sec ⁻¹) Model	$\frac{t}{r}$			$\frac{t}{x_2}$			$\frac{t}{x_1}$
	16.2	22.8	29.5	16.2	22.8	29.5	29.5
A	0.063	0.051	0.039	<0.057	<0.045	<0.034	.100
D	0.163	0.113	0.100	.105	.072	.068	.31
G	.082	.060	.042	.059	.041	.027	.133
E	.214	.158	.099	.140	.104	.068	.215
H	-	-	.172	.177	.144	.109	.30
F	.66	.57	.53	.44	.41	.36	.89
I	.64	.61	.52	.56	.49	.41	.75

t = transition distance
 r = reattachment point distance
 x₁ = minimum pressure point distance
 x₂ = maximum pressure point distance

 (all distances measured from separation point)

Table 1. Ratios Showing Relative Position of Transition

before them, have reported that the beginning of the pressure rise coincided with the transition. (Chapman et. al. on the other hand did illustrate one case where this was not true). However, this was not noted in these experiments (see figure 12 where the transition locations are shown by \downarrow or \uparrow). The cases coming closest to this description are the $\frac{1}{2}$ -inch semicircular cylinder and the truncated airfoil II. The ratio of the distance of the transition to that of the point of minimum pressure is tabulated in the last column of table 1. Oil film studies of the surface flows with some of the models (A, E, G, and H) actually show that the minima of the curves invariably correspond with the point of secondary separation.

The variation of reattachment pressure distribution with the condition of the edge at separation was also investigated and the results, plotted in figure 14, show negligible effect.

Reattachment Pressure Rise (Recovery) Coefficient, σ

From the Korst-Chapman theory and measurements of Moore, some ideas concerning the reattachment pressure rise (or recovery) coefficient, σ , were developed in the "THEORY". The values of σ obtained in the present experiments are given in table 2. Also included is the range of values of σ computed from the results of

U(ft-sec ⁻¹) Model	σ			REMARKS
	16.2	22.8	29.5	
A	> 0.30	> 0.31	> 0.32	Peak pressure not reached.
D	.36	.35	.36	
G	.34	.35	.35	
F	.36	.36	.36	
E	.32	.32	.33	
H	.31	.28	.28	
I	.29	.29	.29	
H*	0.200			
Roshko (Ref. 10)	0.34			
Moore (Ref. 8)	0.109 to 0.32			
Tani (Ref. 11)	0.200 to 0.37			The highest value was obtained with a step of 6 cm. high.
Chapman (Ref. 3)	> 0.35			Peak pressure not reached. (Separation occurred at leading edge of plate upstream of the step.)
Arie and Rouse (Ref. 12)	> 0.30			Peak pressure not reached.

Table 2. Reattachment Pressure Rise Coefficient

Roshko (Ref. 10), Moore (Ref. 8), Tani (Ref. 11), Chapman et. al. (Ref. 3), and Arie and Rouse (Ref. 12). Roshko's results were obtained with a 1-inch circular cylinder placed normal to the flow, and symmetrical to a splitter plate behind; Moore's and Tani's, a backfacing step; Chapman's, a front-facing step²; and those of Arie and Rouse, a flat plate with splitter plate.

These results lend support to the applicability of the Korst-Chapman theory to subsonic problems. Moreover, it may be seen that the cases with higher values of δ_s/h (ratio of the thickness of the free shear layer at separation to the step height) have lower values of σ . Therefore, the value of σ seems to be strongly dependent on δ_s/h .

The findings on σ make one wonder if perhaps all the reattachment pressure distributions may not be put into one series of curves in "reduced" coordinates, with δ_s/h as a parameter. A representation of the curves in such coordinates is shown in figure 15. The ordinate is the "reduced pressure coefficient" defined with respect to separation conditions, i.e.,

2. In this case the separation was at leading edge of the plate forward of the step, and it appears that the reattachment occurred some distance ahead of the step.

$$\begin{aligned}\tilde{C}_p &= \frac{p - p_i}{\frac{1}{2} \rho U_1^2} = \frac{p - p_i}{\frac{1}{2} \rho U_\infty^2} \left(\frac{U_\infty}{U_1}\right)^2 \\ &= \frac{C_p - C_{p_i}}{1 - C_{p_i}}\end{aligned}\quad (3)$$

(since $\left(\frac{U_1}{U_\infty}\right)^2 = 1 - C_{p_i}$, from Bernoulli's Equation.) (It may be noted that $\tilde{C}_{p \max} \equiv \sigma$.) The abscissa is x normalized by the reattachment point distance.

It may be seen that some degree of reduction is obtained, particularly for those cases where $\tilde{C}_{p \max}$ is about 0.35 (corresponding to cases where δ_s/h is small).

Effect of Reynolds Number

In the discussion on "Reattachment Pressure Distributions", it was indicated that there are two categories of flow, one of which is not affected by speed (i.e., Reynolds number) change, and the other which is. The difference between the two lies in whether the transition is close to or far from the reattachment region. Reference is made to table 1, where it may be seen that for forebodies which come under the latter category (F and I), the values of t/r are indeed appreciably greater than the others. Similar observations pertaining to t/x_2 and t/x_1 may be made.

It is of interest that even where there is a

significant effect of Reynolds number on the pressure rise curve, the effect on σ is not very great. This may be seen, for example, for the case of the $\frac{1}{2}$ -inch semicircular cylinder (figure 9) and that of the truncated airfoil II (figure 10).

Transition Reynolds Number

Based on experimental data obtained for Mach numbers as low as 0.40, Chapman et. al. postulated a criterion for "pure laminar separation". "Pure laminar separation" is defined as separated flow which is laminar through the reattachment region. On extrapolating these results to a lower Mach number, one finds that at zero Mach number, the maximum Reynolds number (based on reattachment length) at which the free streamline would remain laminar on reattaching ranges from about 2×10^4 to 6×10^4 . At Reynolds numbers above this, the flow is not expected to be purely laminar.

Table 3 gives a list of Reynolds numbers encountered in these experiments.

In all the cases studied, it may be seen that the Reynolds numbers (based on reattachment length), Re_r , were as low as 11×10^3 , with transition still well upstream of reattachment. A meaningful Reynolds number here would be Re_t , based on transition distance, which was found to be as low as 3×10^3 (Table 3). It may be noted that for the

U(ft-sec ⁻¹) Model	Re _r x 10 ⁻⁴				Re _t x 10 ⁻³		
	16.2	22.8	29.5	46.7	16.2	22.8	29.5
A	6.7	9.2	11.9	-	4.2	4.7	4.6
D	2.3	3.3	4.6	-	3.8	3.8	4.6
G	3.8	5.3	6.8	-	3.1	3.2	2.8
E	3.3	4.8	6.2	-	7.1	7.5	6.2
F	1.1	1.5	1.7	-	7.5	8.5	9.1
H	-	-	8.0	4.5	11.9	13.5	13.7
I	2.2	2.4	2.7	-	13.8	14.9	13.9

Re_r = Reynolds Number based on reattachment point distance

Re_t = Reynolds Number based on transition point distance

(all distances measured from separation point)

Table 3. Reynolds Numbers

longest forebody (I), Re_t reaches its largest values in table 3, about 1.4×10^4 , which approaches the lower Chapman values. It appears that the value of δ_s/h must play a role here, i.e., the larger δ_s/h , the greater is the value of Re_t and also the greater the possible value of Re_r for which laminar reattachment can still be observed. This stems from the fact that the stability of the free shear layer is related to its initial thickness, and the thicker it is, the longer the layer is likely to remain laminar, and the later the transition; i.e., the free shear layer can stay laminar only a certain number of boundary thicknesses after separation.

On the basis of these results and observations about the free shear layer thickness at separation, it is suggested that a more appropriate criterion would be based on some combination of Re_r and δ_s/h , possibly just δ_s/r .

5. CONCLUSION

In the present work, reattachment pressure distributions were obtained for various shapes of forebodies at three or more speeds.

It was found that the values of the reattachment pressure rise coefficient, σ , were about 0.35 as predicted by the Korst-Chapman theory for the cases where the boundary layer thickness at separation, δ_s , was almost zero; and that the greater the value of δ_s/h , the lower the value of σ . It also appears that σ is not dependent on Reynolds number per se, except insofar as it influences δ_s .

Attempts made to reduce all the reattachment pressure distributions into a series of universal curves having δ_s/h as parameter were partially successful. Universality was observed for cases where δ_s was close to zero, but the curves for the other cases deviated by varying degrees depending on the values of δ_s/h and the position of the transition which, in itself, depends on δ_s/h too.

In spite of the fact that the Reynolds numbers (based on reattachment length), Re_r , were as low as 11×10^3 , which is lower than the lowest predicted from the Chapman criterion for "pure laminar separation", none of the cases was observed to have a laminar reattachment. This leads to speculation as to whether a more fundamental parameter might not be used as a criterion, one based on δ_s/h and

Res/Rev.

The results of these experiments do confirm the postulate of Chapman et. al. concerning the importance of the relative locations of the transition and reattachment.

REFERENCES

1. Korst, H.H.; Page, R.H.; Childs, M.E.: Compressible Two-Dimensional Jet Mixing at Constant Pressure. TN 392-1, Univ. of Ill., Eng. Exp. Sta., Mech. Eng. Dept., 1954.
2. Korst, H.H.; Page, R.H.; Childs, M.E.: A Theory for Base Pressures in Transonic and Supersonic Flow. TN 392-2, Univ. of Ill., Eng. Exp. Sta., Mech. Eng. Dept., 1955.
3. Chapman, D.R.; Kuehn, D.M.; Larson, H.K.: Investigations of Separated Flows in Supersonic and Subsonic Streams with Emphasis on the Effect of Transition. NACA TN 3869, 1957.
4. Chapman, D.R.: Laminar Mixing of a Compressible Flow. NACA Rep. 958, 1950.
5. Crabtree, L.F.: The Formation of Regions of Separated Flow on Wing Surfaces. Part I. Low Speed Tests on a Two-Dimensional Wing with a 10% RAE 101 Section. RAE Rep. 2528, 1954.
6. Crabtree, L.F.: The Formation of Regions of Separated Flow on Wing Surfaces. Part II. Laminar Separation Bubbles and the Mechanism of Leading Edge Stall. RAE Rep. 2578, 1957.
7. Moore, T.W.F.: A Note on the Causes of Thin Aerofoil Stall. Journ. Roy. Aero. Soc., Vol. 63 (1959) pp. 724-730.
8. Moore, T.W.F.: Some Experiments on the Reattachment of a Laminar Boundary Layer Separating from a Rearward Facing Step on a Flat Plate Aerofoil. Journ. Roy. Aero. Soc., Vol.64 (1960) pp. 668-672.
9. Roshko, A.: On the Development of Turbulent Wakes from Vortex Streets. NACA Rep. 1191, 1954.
10. Roshko, A.: On the Drag and Shedding Frequency of Two-Dimensional Bluff Bodies. NACA TN 3169, 1954.

REFERENCES - (Cont'd)

11. Tani, I.: Experimental Investigation on Flow Separation over a Step. Paper presented at "Symposium on Boundary Layer Research", Freiburg, Germany. Inst. of Science and Technology, University of Tokyo, Tokyo.
12. Arie, M.; Rouse, H.: Experiments on Two-Dimensional Flow over a Normal Wall. Journ. of Fluid Mech., Vol. 1 (1956), Part 2, pp. 129-141.

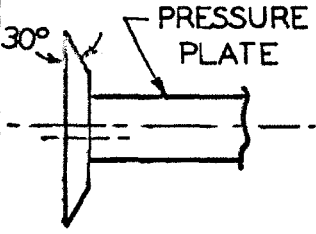
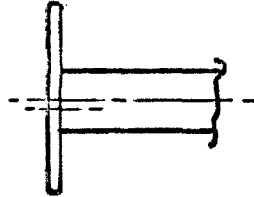
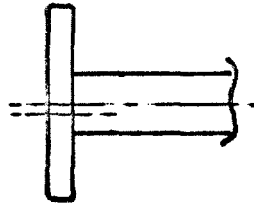
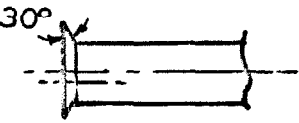
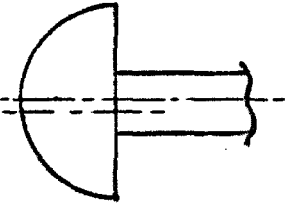
SYMBOL	SHAPE	DESCRIPTION
A		$1 \times \frac{1}{8}$ SHARP EDGED PLATE
B		$1 \times \frac{1}{16}$ BRASS PLATE (STOCK MATERIAL)
C		$1 \times \frac{1}{8}$ AL. PLATE (STOCK MATERIAL)
D		$\frac{1}{2} \times \frac{1}{16}$ SHARP EDGED PLATE
E		1 SEMICIRCULAR CYLINDER

FIG. 1. FOREBODY SHAPES (ALL DIMENSIONS IN INCHES)

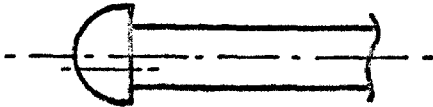
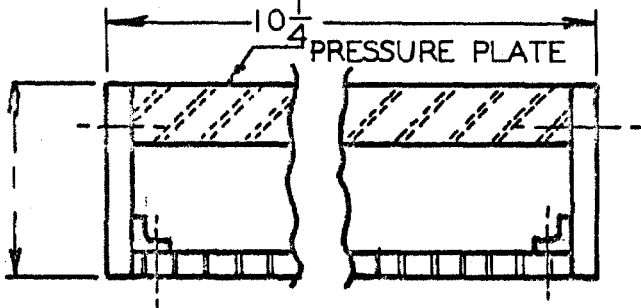
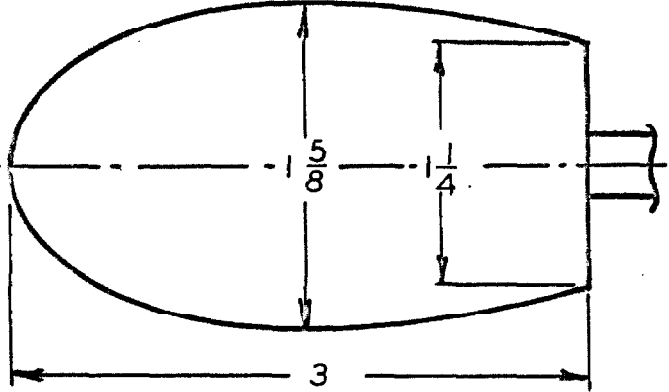
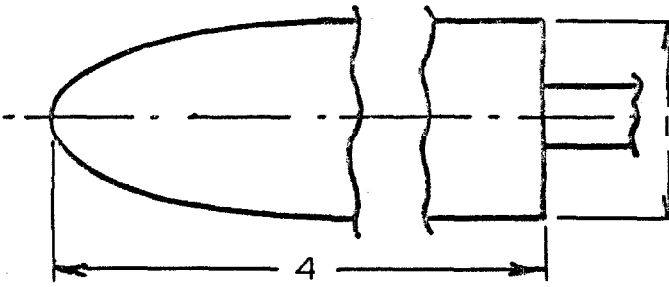
SYMBOL	SHAPE	DESCRIPTION
F		$\frac{1}{2}$ SEMICIRCULAR CYLINDER
G		FLAT NOSE PLATE
H		TRUNCATED AIRFOIL I
I		TRUNCATED AIRFOIL II

FIG. 1 (CONCLUDED). FOREBODY SHAPES (ALL DIMENSIONS IN INCHES)

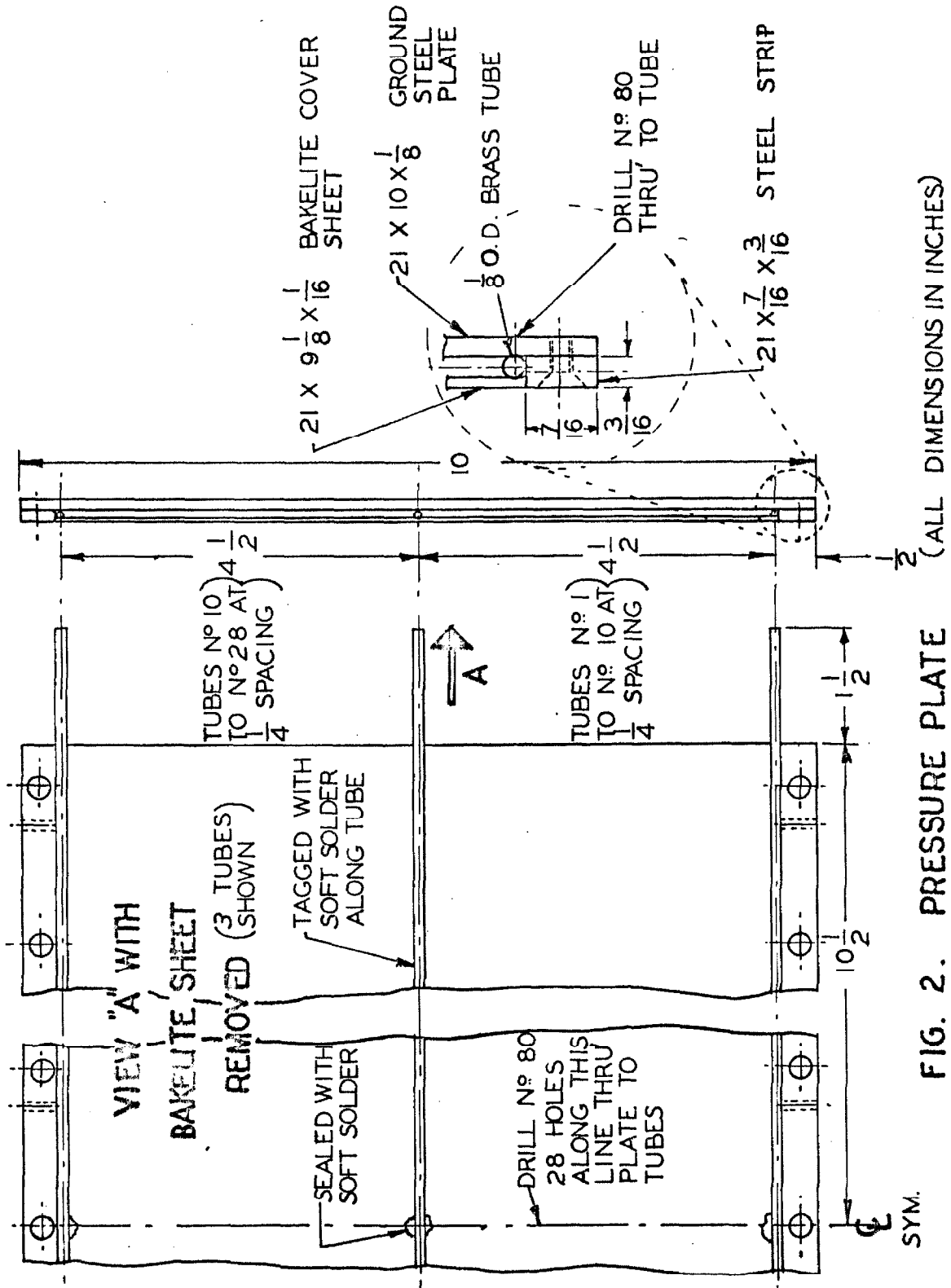
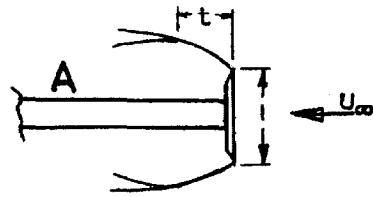
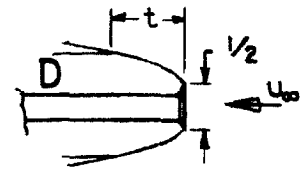


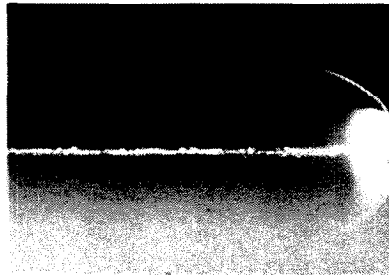
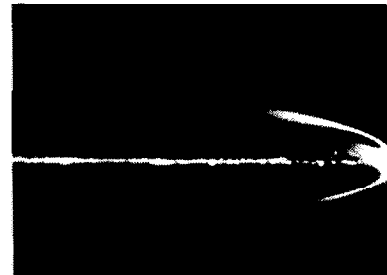
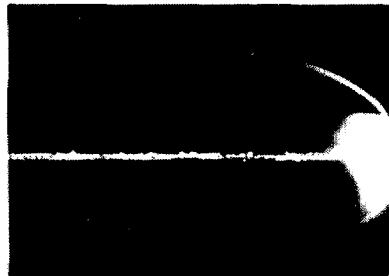
FIG. 2. PRESSURE PLATE



(a)



(b)


 $U_\infty = 16.2, \quad t = 0.55$

 $U_\infty = 16.2, \quad t = 0.48$

 $U_\infty = 22.8, \quad t = 0.44$

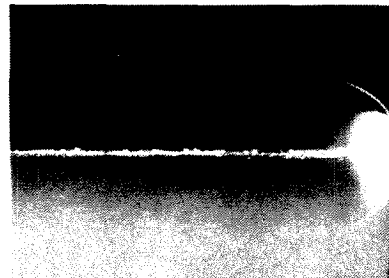
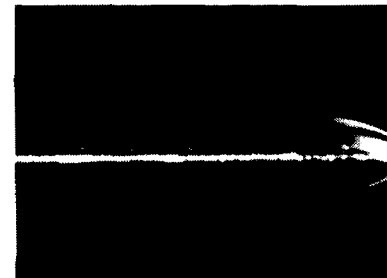
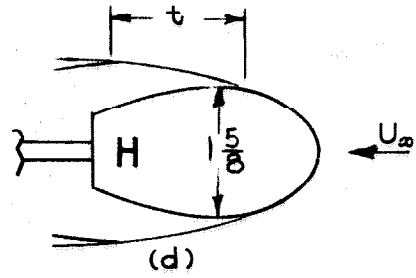
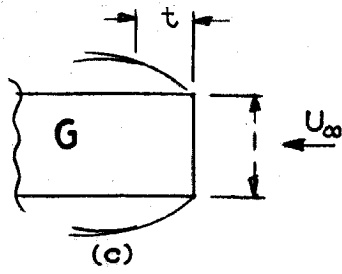
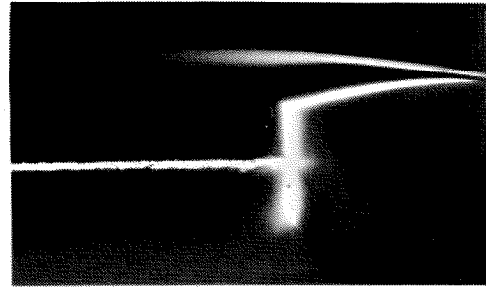
 $U_\infty = 22.8, \quad t = 0.34$

 $U_\infty = 29.5, \quad t = 0.33$

 $U_\infty = 29.5, \quad t = 0.32$

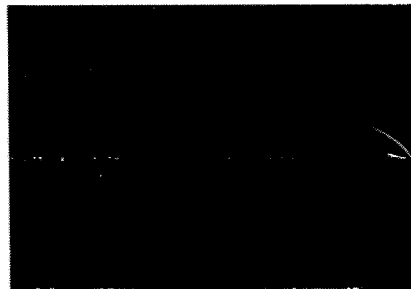
FIG. 3. SMOKE PICTURES SHOWING TRANSITION
 U_∞ IN FT-SEC⁻¹, t IN INCHES



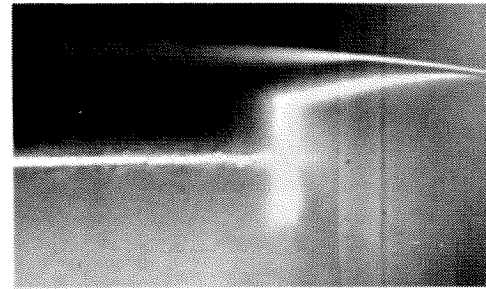
$U_\infty = 16.2$, $t = 0.40$



$U_\infty = 16.2$, $t = 1.51$



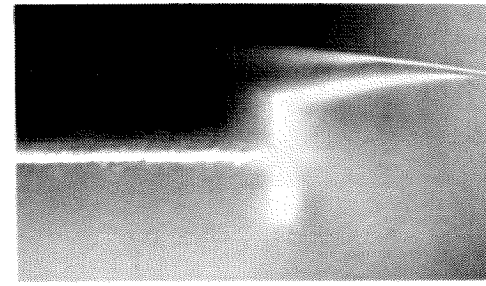
$U_\infty = 22.8$, $t = 0.29$



$U_\infty = 22.8$, $t = 1.22$



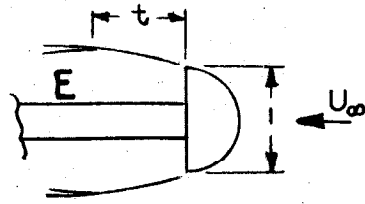
$U_\infty = 29.5$, $t = 0.20$



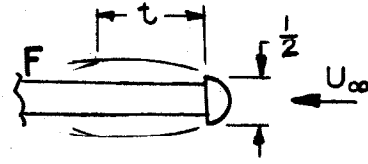
$U_\infty = 29.5$, $t = 0.96$

FIG. 3 CONTINUED

U_∞ IN FT SEC⁻¹, t IN INCHES



(e)



(f)

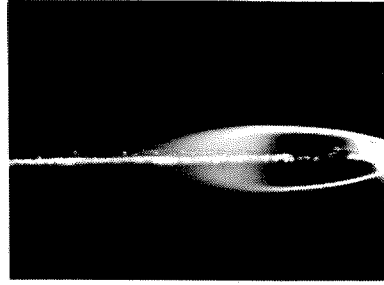
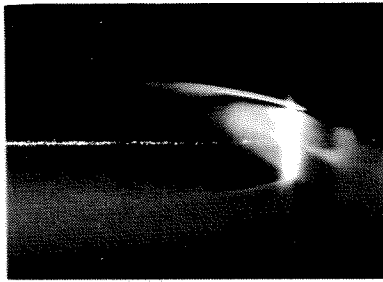
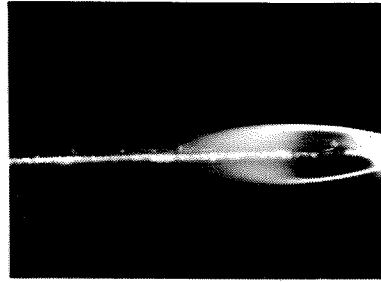
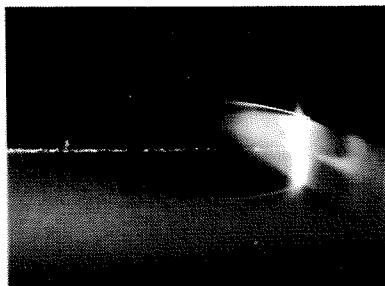
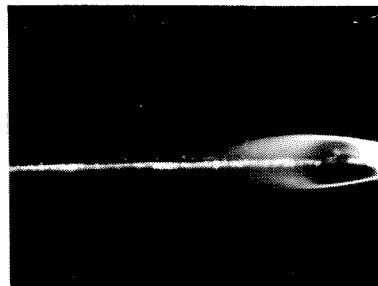
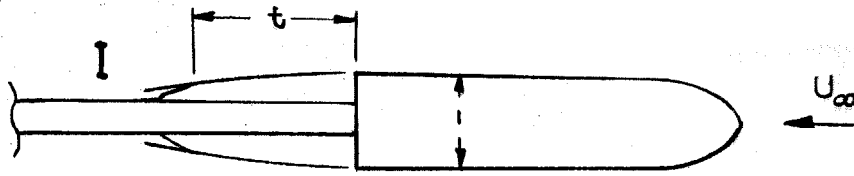
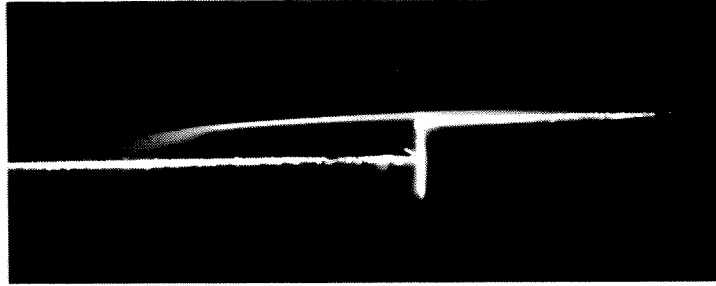
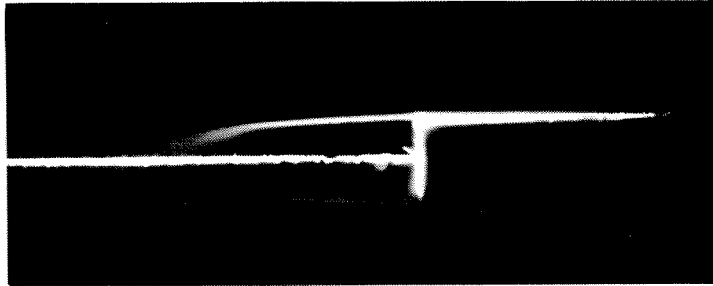
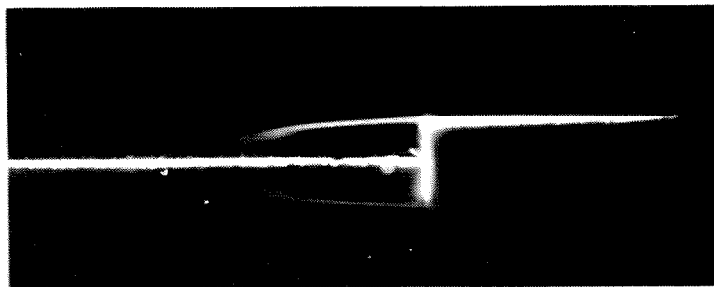

 $U_\infty = 16.2, t = 0.91$

 $U_\infty = 16.2, t = 0.96$

 $U_\infty = 22.8, t = 0.68$

 $U_\infty = 22.8, t = 0.77$

 $U_\infty = 29.5, t = 0.43$

 $U_\infty = 29.5, t = 0.64$

FIG. 3 CONTINUED

U_∞ IN FT SEC⁻¹, t IN INCHES



(g)


 $U_\infty = 16.2$, $t = 1.76$

 $U_\infty = 22.8$, $t = 1.34$

 $U_\infty = 29.5$, $t = 0.97$
FIG. 3 CONCLUDED
 U_∞ IN FT SEC t IN INCHES

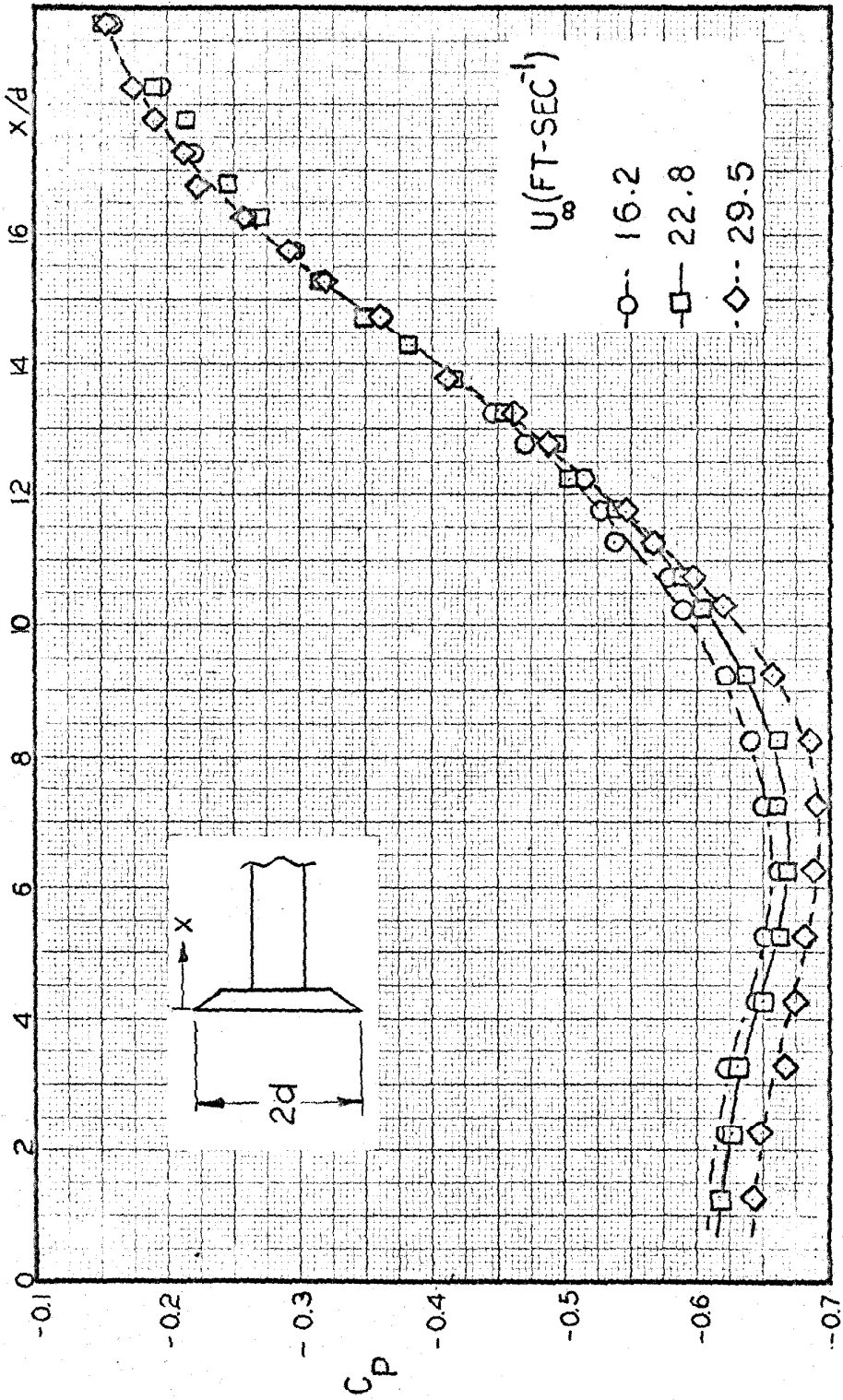


FIG. 4. REATTACHMENT PRESSURE DISTRIBUTION ($2d = 1$ INCH)

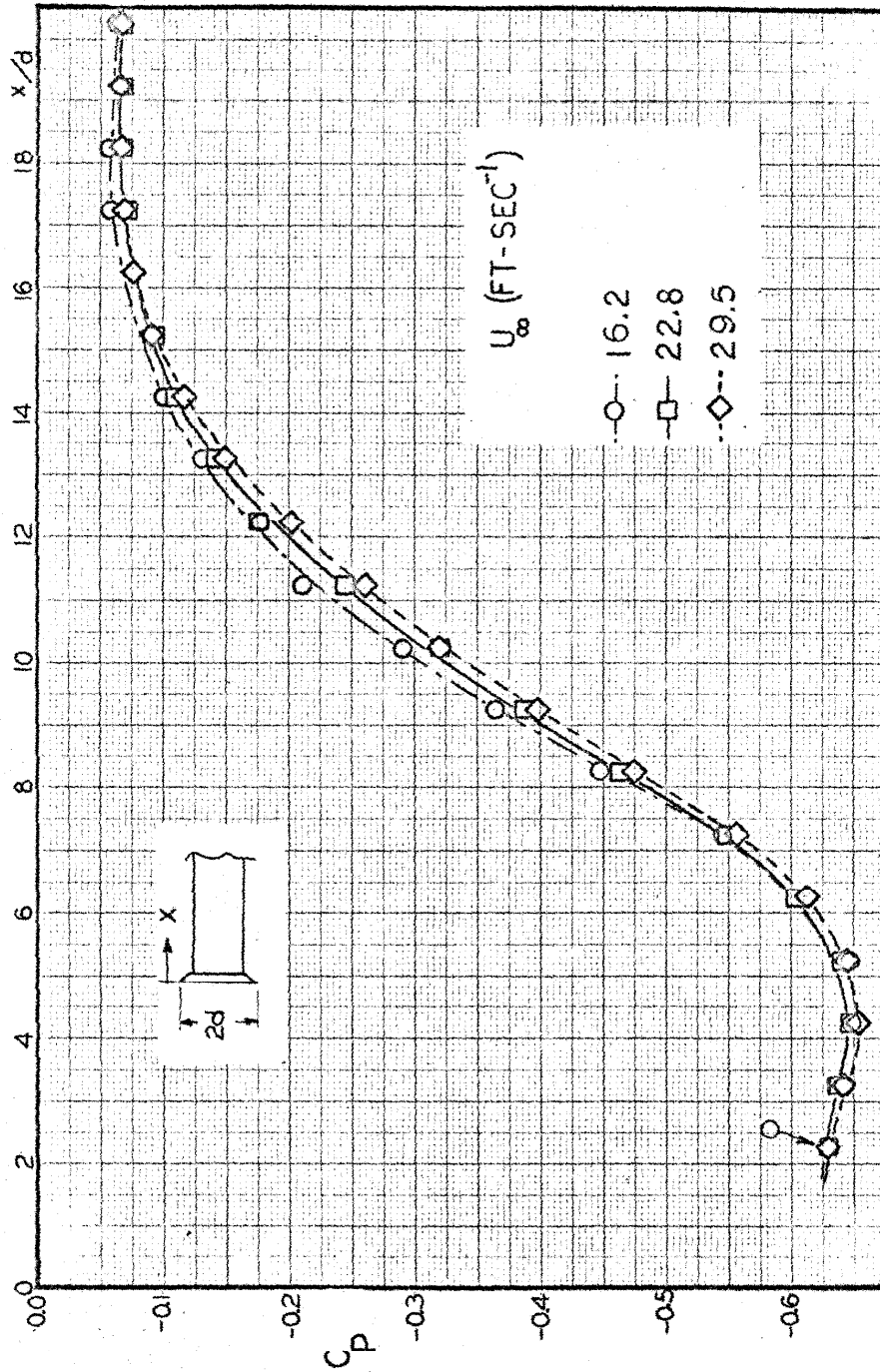


FIG. 5. REATTACHMENT PRESSURE DISTRIBUTION ($2d = 1/2$ INCH)

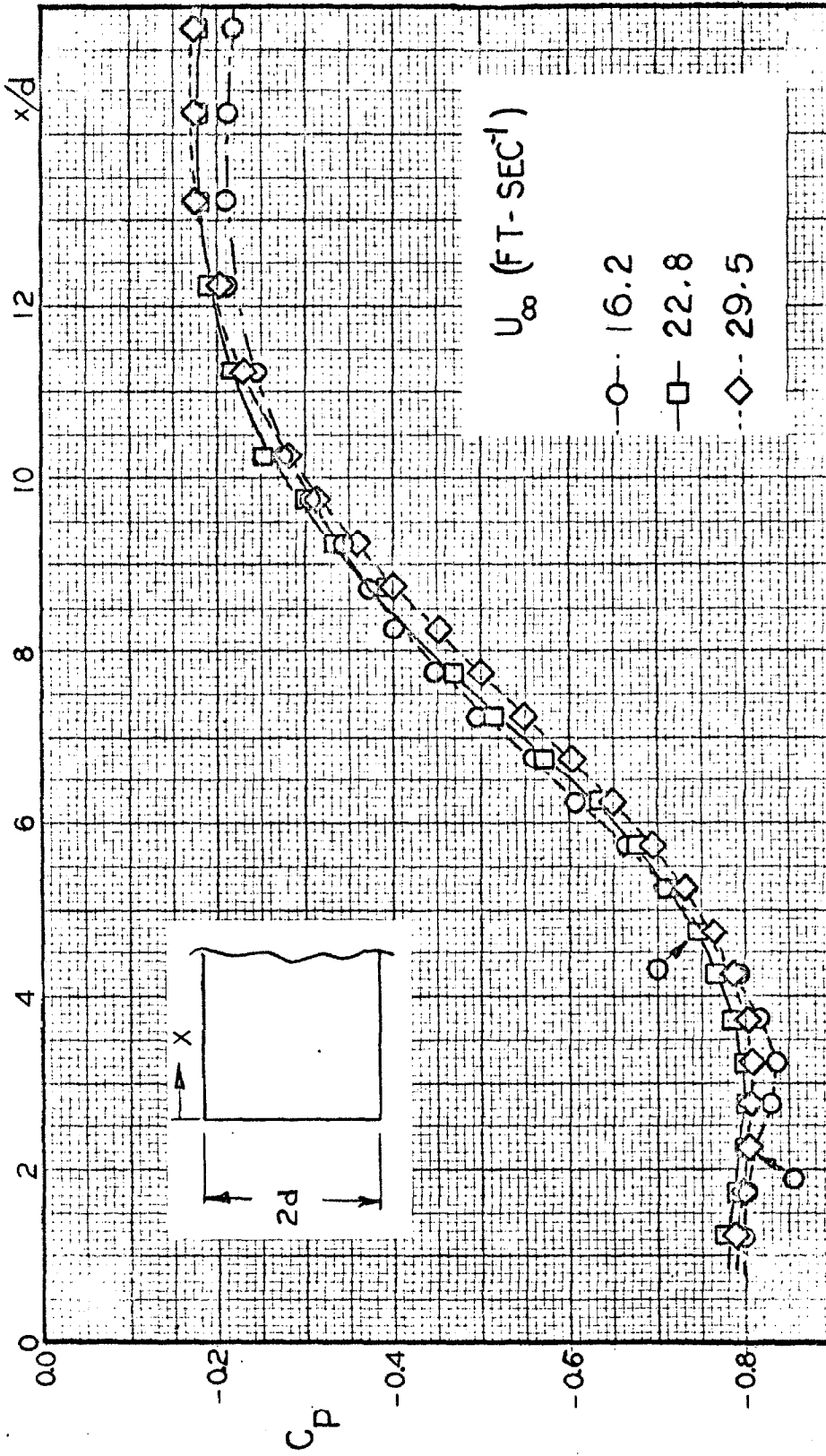


FIG. 6. REATTACHMENT PRESSURE DISTRIBUTION ($2d = 1$ IN.)

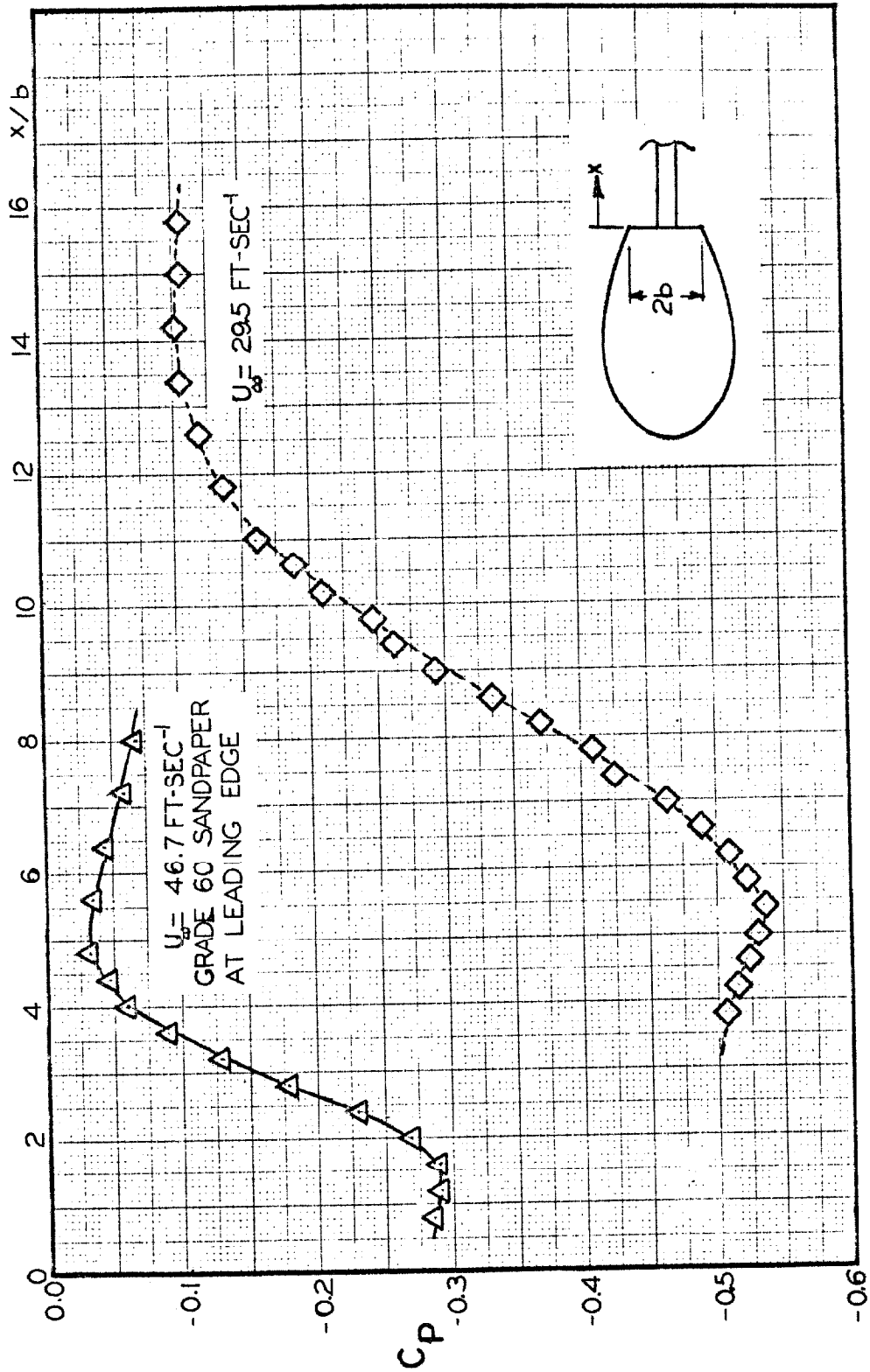


FIG. 7. REATTACHMENT PRESSURE DISTRIBUTION ($2b = 1.25 \text{ IN}$)

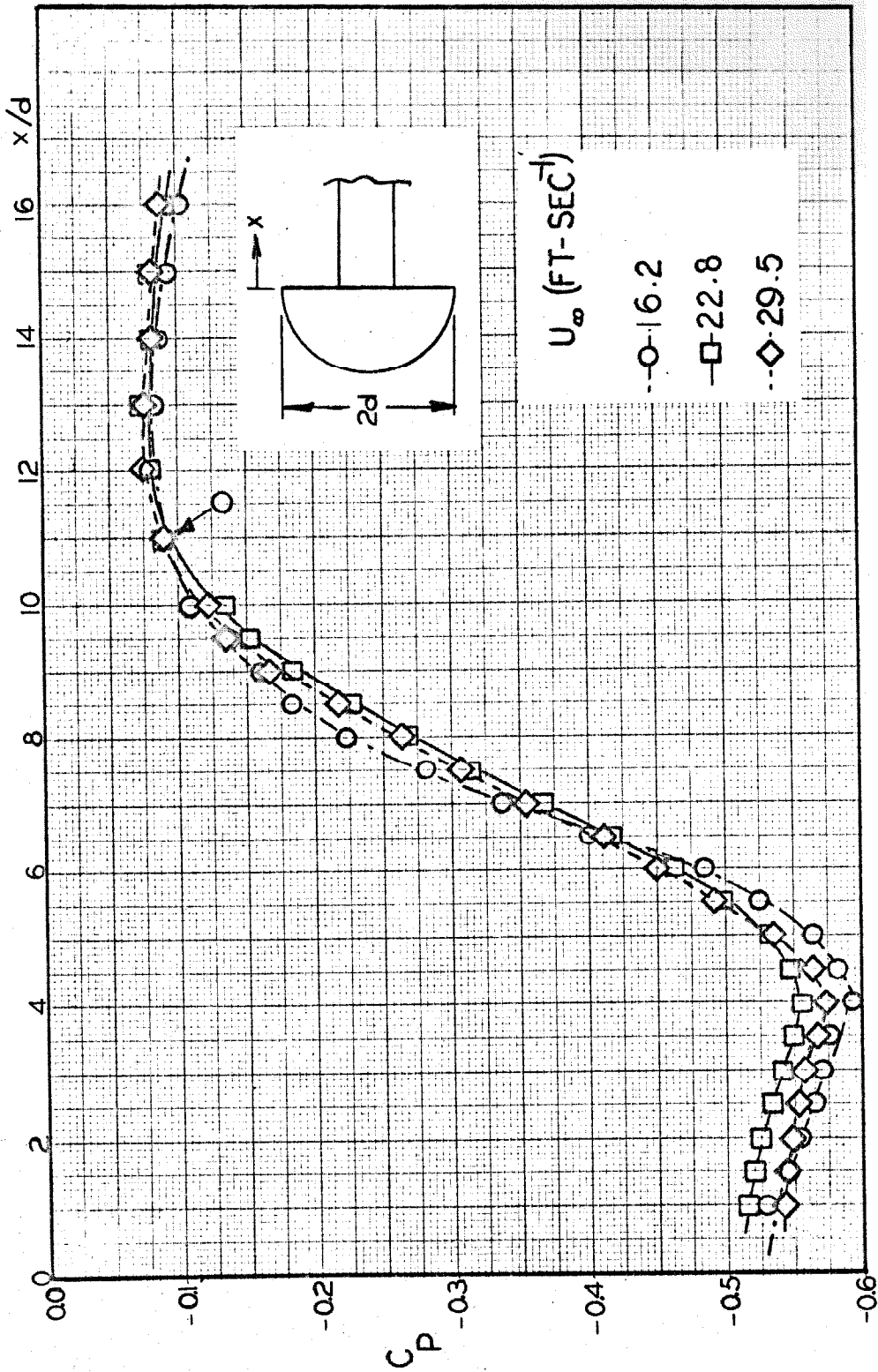


FIG. 8. REATTACHMENT PRESSURE DISTRIBUTION ($2d = 1$ INCH)

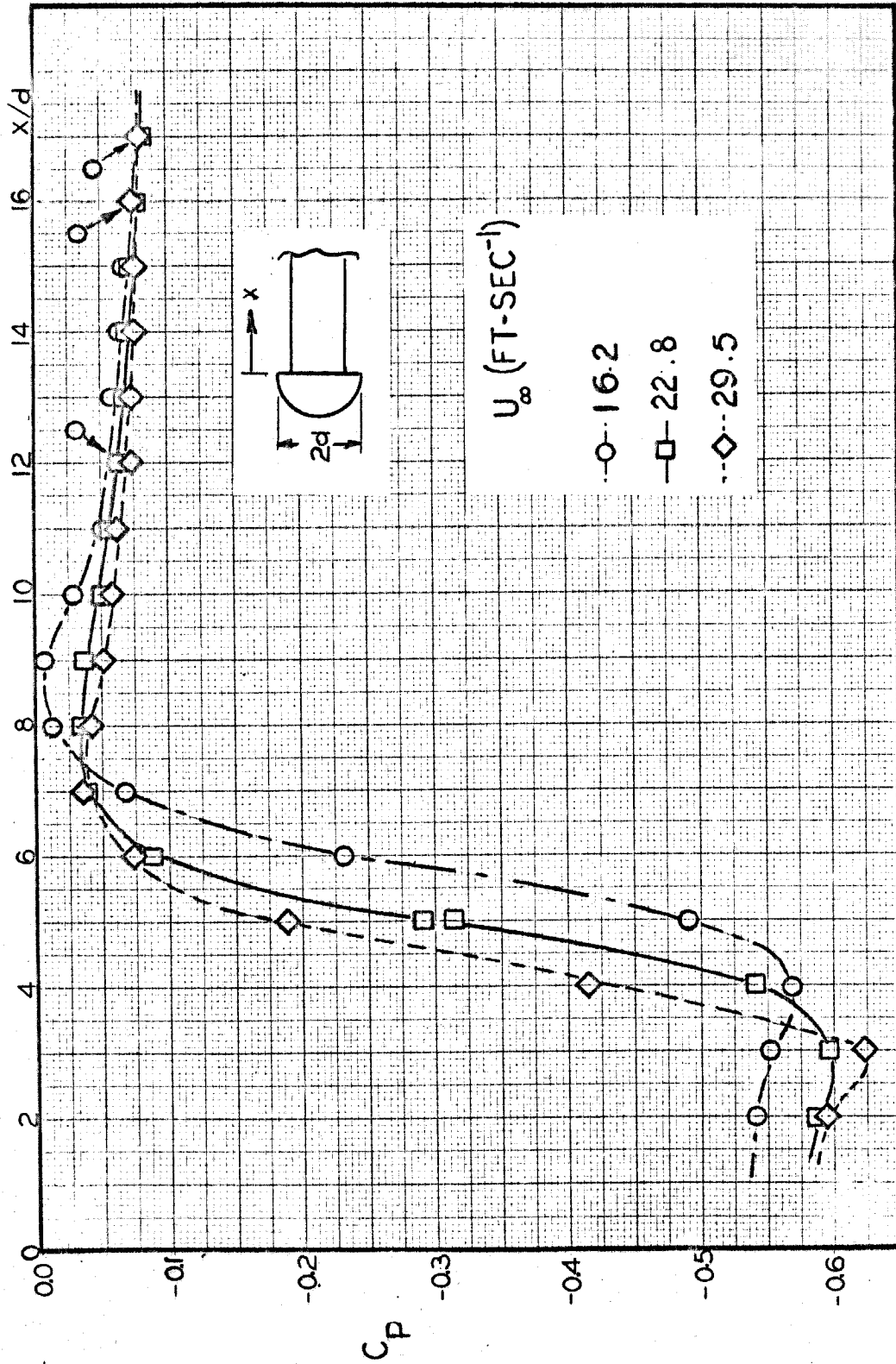


FIG. 9. REATTACHMENT PRESSURE DISTRIBUTION ($2d = 1/2$ IN)

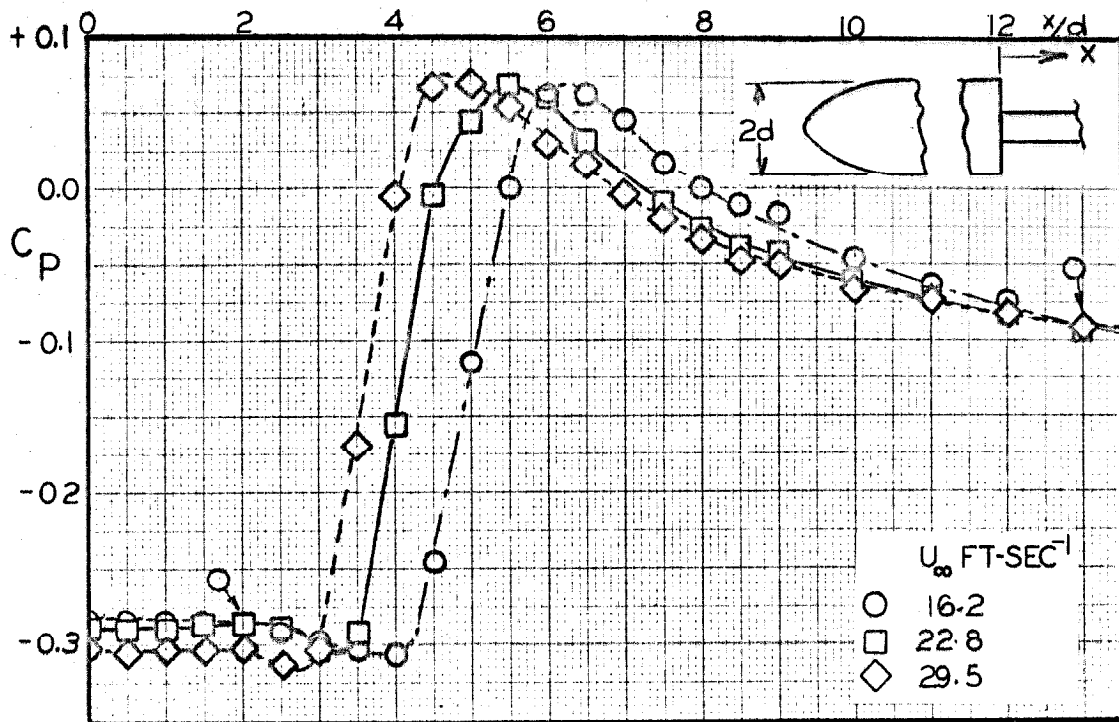


FIG. 10. REATTACHMENT PRESSURE DISTRIBUTION
($2d = 1$ INCH)

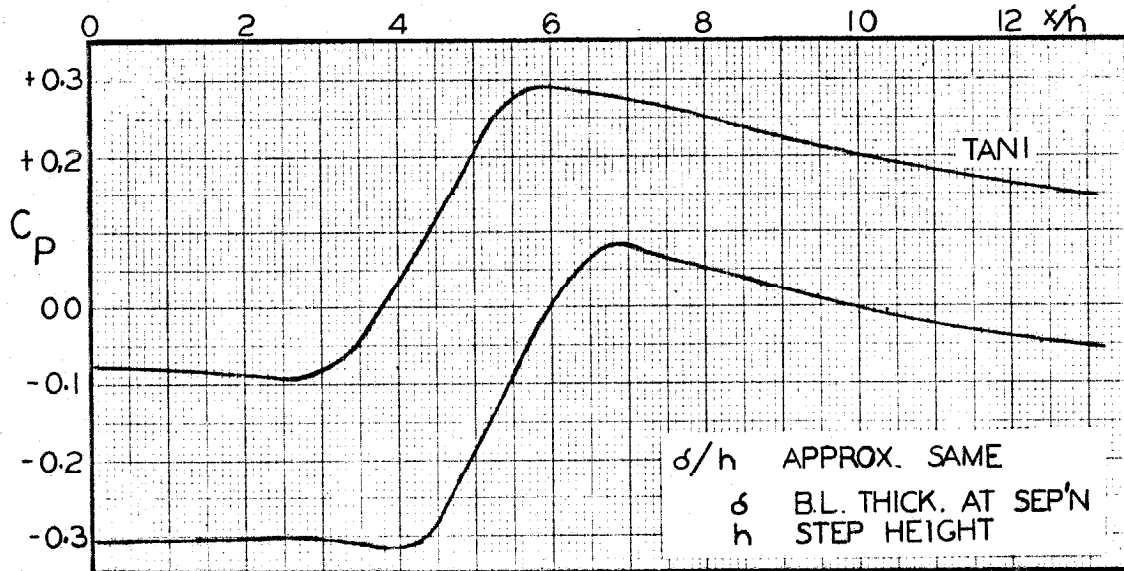


FIG. 11. COMPARISON OF RESULTS OF FIGURE 10 WITH TANI'S [REF. 11]

	U (FT SEC ⁻¹)	h (IN.)
OF FIGURE 10	: 29.5	0.344
WITH TANI'S [REF. 11]	: 32.8	1.57

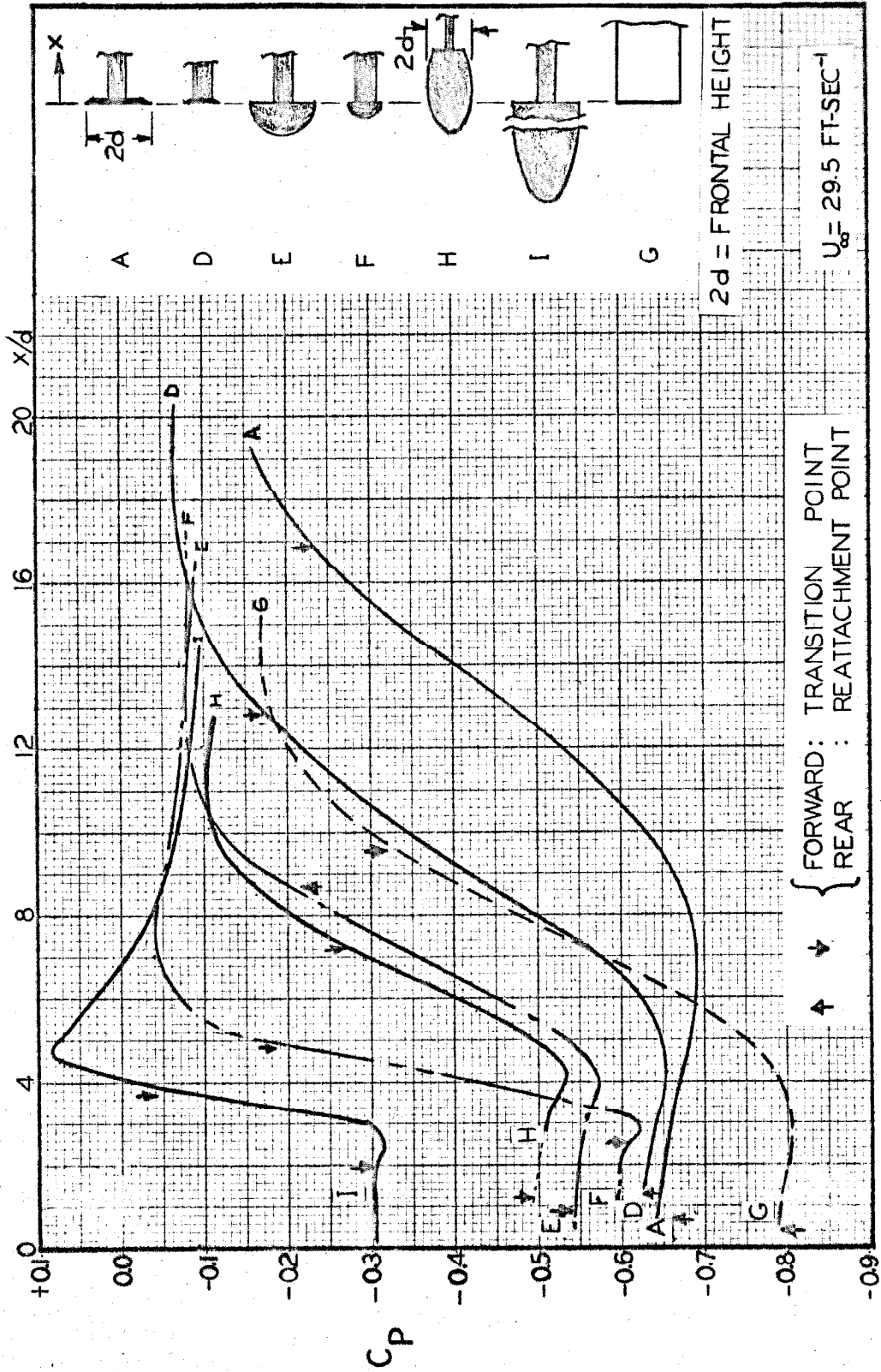


FIG. 12. COMPARISON OF RESULTS FOR VARIOUS SHAPES
 (x NORMALIZED BY 1/2 FRONTAL HEIGHT, d)

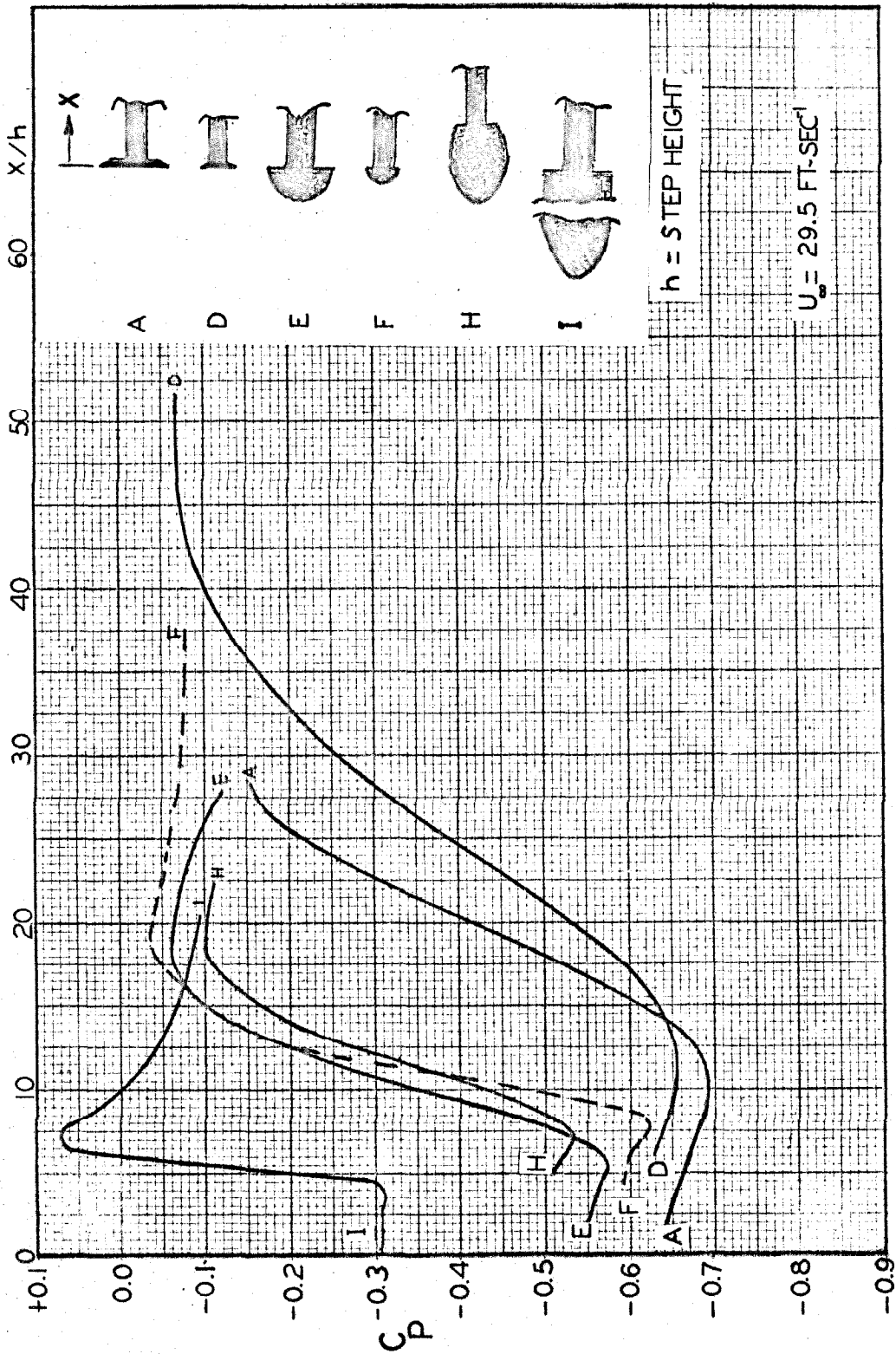


FIG. 13. COMPARISON OF RESULTS FOR VARIOUS SHAPES
(X NORMALIZED BY STEP HEIGHT, h)

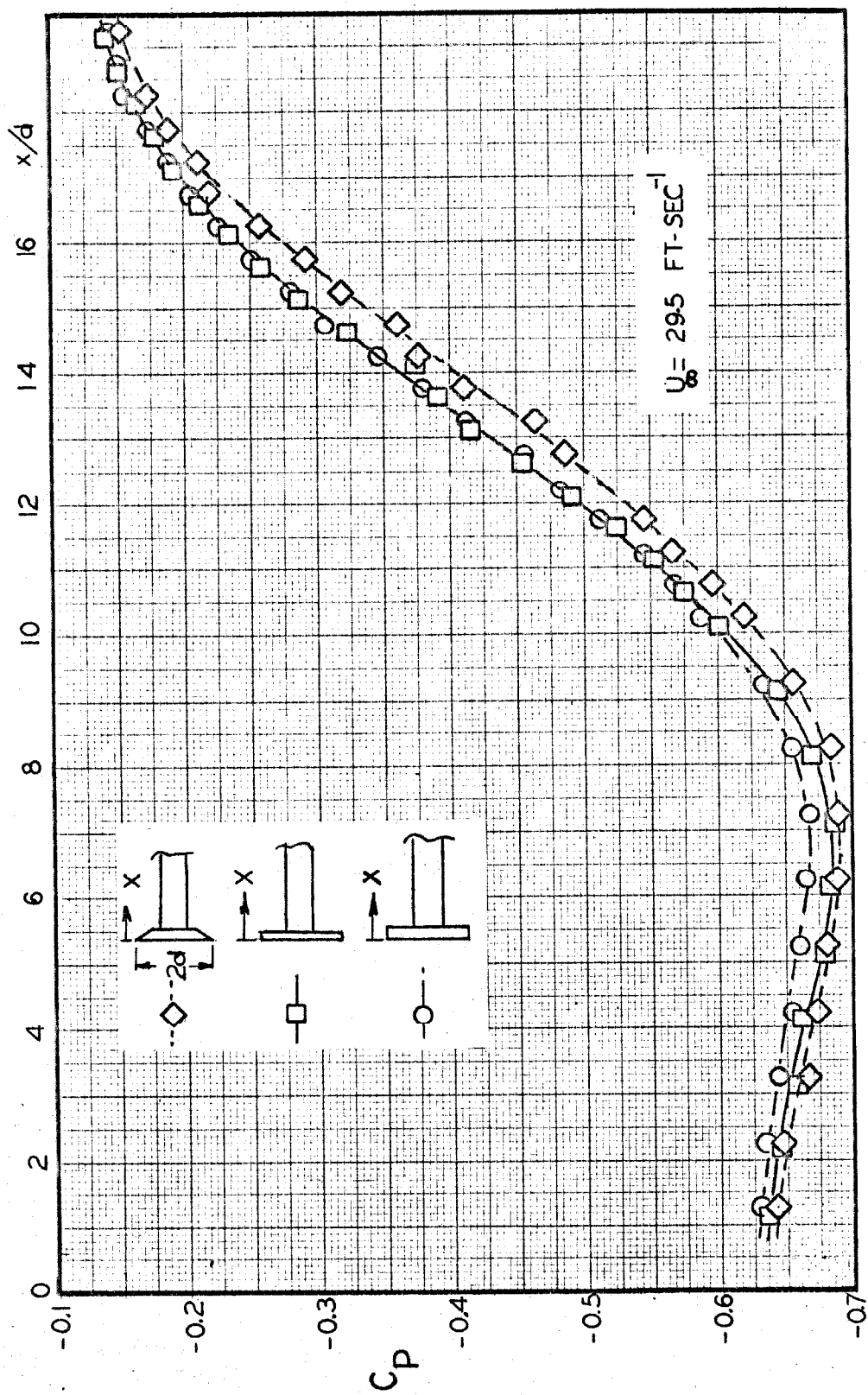


FIG. 14. COMPARISON OF RESULTS FOR 1-INCH PLATES

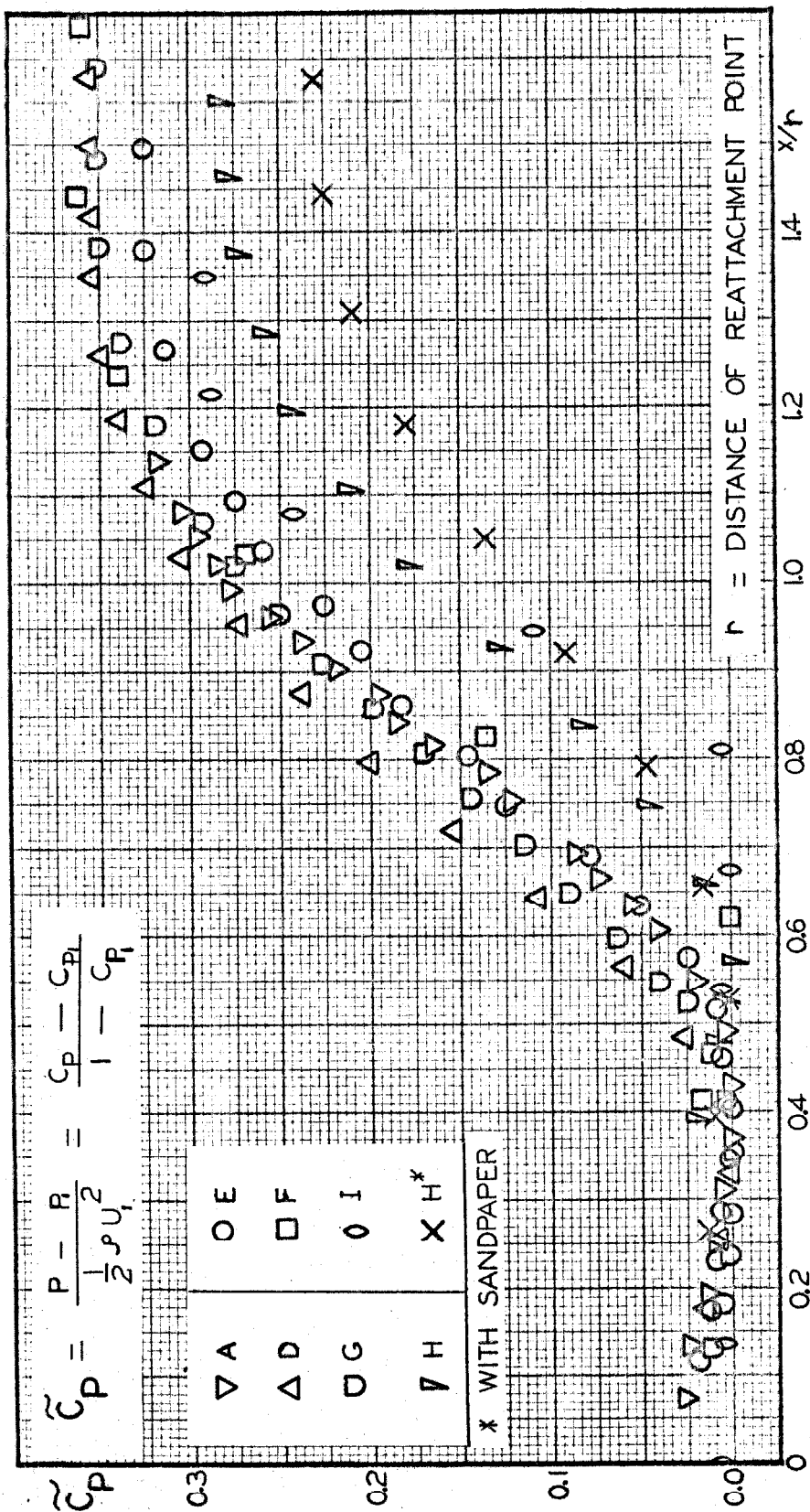


FIG. 15. REATTACHMENT PRESSURE DISTRIBUTION IN REDUCED COORDINATES

$U_\infty = 29.5 \text{ FT SEC}^{-1}$ (EXCEPT H* AT 46.7)